Nondipole parameters in angular distributions of electrons in photoionization of noble-gas atoms

M. Ya. Amusia,[1,2] A. S. Baltenkov,[3,4] L. V. Chernysheva,[2] Z. Felfli,[4] and A. Z. Msezane[4]
[1]*The Hebrew University of Jerusalem, The Racah Institute of Physics, 91904 Jerusalem, Israel*
[2]*Ioffe Physical-Technical Institute, 194021 St. Petersburg, Russia*
[3]*Arifov Institute of Electronics, 700143 Tashkent, Uzbekistan*
[4]*Center for Theoretical Studies of Physics Systems, Clark Atlanta University, Atlanta, Georgia 30314*
(Received 20 September 2000; published 16 April 2001)

The parameters that determine the nondipole $(E1-E2)$ corrections to the photoelectron angular distribution have been investigated for the *s*- and *p*-subshells of the noble-gas atoms through comparing results calculated in the Hartree-Fock (HF) approximation and taking into account multielectron correlations, using the random-phase approximation with exchange. Our results cover the photoelectron energy range ϵ from the photoionization thresholds to 1.6 keV. We find the interesting result that near the photoionization thresholds these parameters are generally characterized by an oscillatory behavior as a function of ϵ, exclusive of the parameter for the He $1s$ subshell. These oscillations are sensitive to multielectron correlations, except those of the Ar $3p$ subshell. This finding supports once more that the photoprocesses in these atomic subshells are of a collective character. We conclude that their correct description cannot be achieved within the framework of a one-electron approximation such as the HF approximation. Results are presented and discussed.

DOI: 10.1103/PhysRevA.63.052506 PACS number(s): 31.25.−v, 32.80.Dz, 32.80.Fb

I. INTRODUCTION

The angular distribution of the electrons ejected in atomic photoionization is an important source of information on the inner atomic structure and the dynamics of the process. The angular differential cross sections in contrast to the total cross sections are more sensitive to the coupling among the atomic electrons. Thus, they provide a stringent test of theory when its results are compared with those from measurement. Until recently the possibility of studying the atomic photoionization process was limited mainly by the low intensity of the ultraviolet and x-ray radiation sources and the impossibility of varying the radiation frequencies over a sufficiently wide range. In fact, not too long ago major experiments in this field were performed using discrete lines from x-ray tubes [1–3]. The experimental and theoretical studies at that time concentrated mainly on the investigation of the individual subshell contributions to the total atomic photoionization cross sections.

Nowadays, very intense tunable and highly polarized photon beams produced by synchrotrons and electron storage rings make it possible to study also the angular distribution of photoelectrons in great detail. Modern photoelectron spectroscopy facilities allow the measurement of both differential and total photoionization cross sections of individual atomic subshells. For several years a number of experiments in the field of atomic photoionization focused on the measurement of the nondipole terms in the photoelectron angular distributions [4–8], although the deviation from the dipole angular distributions of photoelectrons was observed much earlier [9]. However, the data were obtained at relatively high photon frequencies ω's. It is clear that the experimentalists will soon move to the much more interesting low ω domain where the role of interelectron interaction is larger but the nondipole parameters themselves are smaller than at high ω. Therefore, theoretical predictions in this regime are important, interesting, and timely.

The one-electron approach used in the calculations of nondipole parameters [10,11] proved to be insufficient to describe recent experimental findings [12]. In this experiment the dipole and nondipole asymmetry parameters of the angular photoelectron distribution in the $2p$ photoionization of Ne was measured. The measured results for the dipole parameter are in good agreement with other experimental data obtained in [13]. But the values of the nondipole asymmetry parameters are one-and-a-half-times higher than those of the one-electron Hartree-Slater prediction [10]. In order to explain this disagreement, the multielectron correlations in Ne were taken into account in recent papers [14,15]. Using only the random-phase approximation with exchange (RPAE) the experimental data [12] were described satisfactorily. The same approximation was used in [16] to calculate the asymmetry parameters for the *s* subshells of some atoms and also in papers [17–19] to describe the behavior of the nondipole angular asymmetry parameters in the vicinity of quadrupole and dipole autoionizing resonances.

Although some calculations of the nondipole parameters were performed beyond the framework of the one-electron approximation, these were carried out nonsystematically. The aim of this paper is to fill a gap in this field. We will attempt to shed light upon the influence of multielectron correlations as a function of the frequency on the nondipole asymmetry parameters, starting from the ionization thresholds. Quite often the one-electron approximation is incapable of describing even the total photoionization cross section of the outer subshells of multielectron atoms, not to mention the differential cross section. This is connected with the fact that the photoionization of outer atomic subshells has, as a rule, a collective character. With this in mind, we will calculate the nondipole parameters for the outer *s* and *p* subshells of the noble-gas atoms, where correlation effects are expected to be strong. Consequently, we shall use the one-electron Hartree-Fock approximation as a first step and then take into account the multielectron correlations in the framework of the RPAE.

As is known the latter approximation has been successful in calculating the dipole photoionization cross sections and the angular asymmetry parameter for the outer and intermediate subshells of numerous atoms [20].

In this paper we report calculated results of the nondipole asymmetry parameters obtained in the one-electron Hartree-Fock approximation (HFA) and in the RPAE for the atomic subshells: He($1s$), Ne($2s,2p$), Ar($3s,3p$), Kr($4s,4p$), and Xe($5s,5p$). The results cover the photon-energy range from the outer s and p subshell thresholds to about 1.6 keV. Sections II and III deal with the theory and results, respectively, while Sec. IV presents the conclusion and discussion.

II. THEORY

A. Overview

Theoretical calculations of the nondipole effects in the low photon-energy region can be performed using a nonrelativistic approach. Then the amplitude of the atomic photoionization is proportional to the modulus squared of the matrix element [21]

$$M_{if}=\langle f|(\vec{e}\cdot\vec{p})\exp(i\vec{\kappa}\cdot\vec{r})|i\rangle, \tag{1}$$

where $|i\rangle$ and $|f\rangle$ are the initial and final atomic states, respectively, and $\vec{\kappa}$ and $\vec{e}$ are the photon momentum and polarization vector, $\vec{r}$ is the electron coordinate, and $\vec{p}$ is its momentum operator. Modern understanding of the low-energy atomic photoeffect is largely based on the dipole approximation [20–23]. For frequencies satisfying the condition $\kappa c\cong\omega a/c\ll 1$, where a is the radius of the ionized atomic subshell and c is the velocity of light, the photon interaction with the atomic electron becomes purely electric dipole ($E1$). In this case, where the exponent in Eq. (1) is replaced by unity, the values of the photoelectron orbital angular momenta in the final state are determined by the dipole selection rule $\Delta l=\pm 1$. The interference between the corresponding photoelectron waves leads to the general formula for the angular distribution of photoelectrons [24].

For high photon energies the dipole approximation is no longer valid [25,26]. The inclusion of retardation, i.e., the $\exp(i\vec{\kappa}\cdot\vec{r})$ factor in the photon-electron interaction leads to the asymmetry of the differential cross section. Although the retardation correction to the dipole angular distribution can be calculated correctly in the nonrelativistic approximation with an accuracy of up to the terms of the first order in $\vec{\kappa}$ [25,26], the corrections of the second and higher orders are accounted for only in the fully relativistic approach [27]. To calculate the first retardation correction in the nonrelativistic approximation, i.e., the nondipole correction to the differential cross section for photoionization, Eq. (1) must be rewritten as [21]

$$M_{if}=\langle f|(\vec{e}\cdot\vec{p})[1+(i\vec{\kappa}\cdot\vec{r})]|i\rangle. \tag{2}$$

The second term in Eq. (2) term defines the amplitudes of magnetic-dipole ($M1$) and electric-quadrupole ($E2$) transitions. The interference of the $E1$, $M1$, and $E2$ amplitudes leads to a more complicated general form of the photoelectron angular distribution [28,29]. In this case the nondipole corrections to the atomic photoeffect cross section are the results of interference between the $E1$ and $E2$ electron transitions from the initial atomic state to the continuum final state.

To describe the observed [2,3] deviations from the dipole angular distributions for Kr at lower photon energies (0.3 to 1.5 keV) hydrogenlike wave functions were used [30] for the $3s$, $3p$, and $3d$ electrons of Kr. Within the one-electron relativistic central-field approximation the differential cross section for unpolarized radiation is given by [31–33]

$$\frac{d\sigma_{nl}(\omega)}{d\Omega}=\frac{\sigma_{nl}(\omega)}{4\pi}\Sigma_n B_n P_n(\cos\vartheta), \tag{3}$$

where $\sigma_{nl}(\omega)$ is the total photoionization cross section of the nl atomic subshell and $P_{nl}(\cos\theta)$ are the Legendre polynomials. The relativistic approximation can also be used to describe the differential cross section for photoionization at lower energy [34]. Then Eq. (3) reduces to [35]

$$\frac{d\sigma_{nl}(\omega)}{d\Omega}=\frac{\sigma_{nl}(\omega)}{4\pi}\left[1-\frac{\beta(\omega)}{2}P_2(\cos\vartheta)\right], \tag{4}$$

where $\beta(\omega)$ is defined by the dipole matrix elements $D_{l\pm 1}$ and the phase shifts $\delta_{l\mp 1}$ of the photoelecton wave functions. The replacement in Eq. (4) of $-\beta(\omega)/2$ by $\beta(\omega)$ describes the differential cross section by polarized incident light. In this case ϑ is the angle between the direction of the polarization and the direction of the photoelectron.

The general expression for the differential cross section for photoionization by unpolarized light, including the lowest-order $E1-E2$ interference corrections, is given by [36,37]

$$\frac{d\sigma_{nl}(\omega)}{d\Omega}=\frac{\sigma_{nl}(\omega)}{4\pi}\left[1-\frac{\beta(\omega)}{2}P_2(\cos\vartheta)+\kappa\gamma(\omega)P_1(\cos\vartheta)+\kappa\eta(\omega)P_3(\cos\vartheta)\right]. \tag{5}$$

The expression for the nondipole angular distribution parameters and via dipole and quadrupole matrix elements and phase shifts of the photoelectron wave function in the continuum were obtained [36,37]. For linearly polarized radiation the corresponding formulas were also derived in papers [38,39,10]

$$\frac{d\sigma_{nl}(\omega)}{d\Omega}=\frac{\sigma_{nl}(\omega)}{4\pi}\{1+\beta(\omega)P_2(\cos\vartheta)+[\delta^C(\omega)+\gamma^C(\omega)\cos^2(\vartheta)]\sin\vartheta\cos\Phi\}. \tag{6}$$

Here ϑ is the polar angle of the photoelectron velocity $\vec{v}$ with respect to the photon polarization vector $\vec{e}$, and Φ is the azimuthal angle defined by the projection of $\vec{v}$ in the plane perpendicular to $\vec{e}$ and containing the photon propagation

vector $\vec{\kappa}$. The nondipole asymmetry parameters $\gamma^C(\omega)$ and $\delta^C(\omega)$, introduced in [10], are connected to $\gamma(\omega)$ and $\delta(\omega)$ of Eq. (5) by the following relations:

$$\gamma^C/5+\delta^C=\kappa\gamma, \quad \gamma^C/5=-\kappa\eta. \tag{7}$$

Formulas for nondipole parameters and expressions similar to Eqs. (5) and (6) were also derived in Ref. [11]. The extension to nonrelativistic calculations of the first-order retardation corrections to the angular distribution for the *s* and *p* atomic subshells were performed [10,11]. The general formula for the angular distribution for the case of arbitrary photon polarization was derived [40]. Recently, the nondipole asymmetry parameters for Ar $1s$, Kr $2s$, and $2p$ subshells were measured at photon energies of 2–3 keV above their respective thresholds [41]. These measurements focused on the core levels of the noble gases and started detailed investigations of the nondipole asymmetry parameters $\gamma^C(\omega)$ and $\delta^C(\omega)$ in the angular photoelectron distributions given by Eq. (6). The measurements of the nondipole parameters for the inner atomic subshells agreed with the calculations [10,11].

B. General formulas for nondipole asymmetry parameters

The expressions for the nondipole asymmetry parameters $\gamma^C(\omega)$ and $\delta^C(\omega)$ involving dipole and quadrupole matrix elements and photoelectron phase shifts in the case of an arbitrary orbital angular momentum *l* of a bound electron are rather complicated and can be found in [10,36–39]. In this paper we present only the expressions of interest, for *s* and *p* atomic subshells. In the single-electron approximation for the *s* subshell one has

$$\delta_s^C=0 \quad \text{and} \quad \gamma_s^C(\omega)=6\kappa\frac{q_2}{d_1}\cos(\delta_2-\delta_1). \tag{8}$$

For the *p* subshell the δ^C parameter is of the form

$$\delta_p^C=\frac{3\kappa}{5[d_0^2+2d_2^2]}\{d_0[q_1\cos(\delta_1-\delta_0)+q_3\cos(\delta_3-\delta_0)] + d_2[q_1\cos(\delta_1-\delta_2)+q_3\cos(\delta_3-\delta_2)]\}, \tag{9}$$

while the γ^C is given by the expression

$$\gamma_p^C=\frac{3\kappa}{5[d_0^2+2d_2^2]}\{-5d_0q_3\cos(\delta_3-\delta_0) + 2d_2[2q_3\cos(\delta_3-\delta_2)-3q_1\cos(\delta_1-\delta_2)]\}. \tag{10}$$

In these formulas q_i and d_i are the quadrupole and dipole radial matrix elements of the transition between one-electron initial $ns(p)$ states and the corresponding states of the continuous spectrum ϵl, where ϵ is the photoelectron energy and *l* is the angular momentum of an electron in the final state; $\delta_i(\epsilon)$ are the phase shifts of the photoelectron wave functions in the continuum.

The dipole and quadrupole matrix elements are determined by the radial integrals

$$d_1=\int P_{ns(p)}(r)rP_{\epsilon l}(r)dr \quad \text{and}$$

$$q_2=\tfrac{1}{2}\int P_{ns(p)}(r)r^2P_{\epsilon l}(r)dr, \tag{11}$$

with $P_{ns(p)}(r)/r$ and $P_{\epsilon l}(r)/r$ being the radial parts of the one-electron wave functions of the $ns(p)$ subshells and the continuum spectrum, respectively. In order to take into account the multielectron correlations, we have to generalize the formulas for the nondipole parameters. The dipole and quadrupole matrix elements will be calculated in the framework of the RPAE [20]. The procedure of solving the RPAE equations for the dipole transition is discussed in [42]. For the quadrupole matrix elements a similar procedure is used. Symbolically, the RPAE equations for the matrix elements D_i and Q_j can be written in the form

$$\hat{D}_i=\hat{d}_i+\hat{U}_1\hat{\chi}_1D_i \quad \text{and} \quad \hat{Q}_j=\hat{q}_j+\hat{U}_2\hat{\chi}_2Q_j, \tag{12}$$

where $\hat{d}(\hat{q})$ are the dipole (quadrupole) photon-absorption operators in the one-electron approximation, $\hat{U}_1$ ($\hat{U}_2$) are the dipole (quadrupole) components of a combination of the direct and exchange Coulomb interelectron interaction. The operators $\hat{D}$ ($\hat{Q}$) and $\hat{d}$ ($\hat{q}$) describe the elimination of an electron from the atom, i.e., the creation of an electron-hole pair. The operators $\hat{\chi}_1$ ($\hat{\chi}_2$) describe the propagation of the initially created (or any other connected to it by the Coulomb interelectron interaction) electron-hole pair. Again, symbolically, $\hat{\chi}_1$ ($\hat{\chi}_2$) can be expressed as

$$\hat{\chi}_{1(2)}=\frac{\hat{1}}{\omega-\epsilon_{1(2)}-i\eta}-\frac{\hat{1}}{\omega+\epsilon_{1(2)}}. \tag{13}$$

Here $\epsilon_{1(2)}>0$ is the energy of an intermediate electron-hole state excited through a dipole (quadrupole) transition.

In Eq. (12), the summation over the intermediate discrete states and the integration over the continuum states are performed. The imaginary parts of the *D* and the *Q* matrix elements come from the fact that the energy denominator of the first term of Eq. (13) can reach zero as indicated below. The behavior near this singularity is defined by introducing the infinitesimal imaginary term $i\eta$. The first term in Eq. (13) can be expressed as

$$\frac{1}{(\omega-\epsilon_{1(2)}-i\eta)}=\mathrm{P}\frac{1}{(\omega-\epsilon_{1(2)})}+i\pi\delta(\omega-\epsilon_{1(2)}) \tag{14}$$

where P denotes the principal value of the integral. According to Eq. (14), the dipole and quadrupole matrix elements in the RPAE become complex values: $D_i=D_i'+iD_i''$ and $Q_j=Q_j'+iQ_j''$ respectively. As was shown in [36,37], in order to generalize the formulas for the nondipole parameters it is necessary to replace in Eqs. (8)–(10) the matrix elements d_i and q_j by D_i and Q_j, respectively. The nondipole param-

eters, in this case, are described by expressions similar to those in Eqs. (8)–(10), but with the following substitutions:

$$d_i^2 \rightarrow |D_i'|^2 + |D_i''|^2,$$

and

$$d_i q_j \cos(\delta_j - \delta_i) \rightarrow (D_i' Q_j' + D_i'' Q_j'')\cos(\delta_j - \delta_i) - (D_i' Q_j'' - D_i'' Q_j')\sin(\delta_j - \delta_i). \quad (15)$$

Formulas (6)–(8) and (12)–(15) will be used in Sec. III to calculate the nondipole asymmetry parameters. Note that in Eq. (15) only terms of order k are retained so that terms of order $|Q_j|^2$ are neglected.

III. NUMERICAL RESULTS

Before we present the results of our calculations, we note that the experimental procedure for measuring the nondipole parameters for linearly polarized photons consists of recording the number of photoelectrons ejected at definite angles and relative to the photon polarization vector [6,7]. The particular choice of a ''magic polar angle'' in these experiments permits the measurement of the nondipole parameter γ^C for s subshells and the combination $\gamma^C + 3\delta^C$ for atomic subshells with $l > 0$. Therefore only the quantities γ_s^C and $\gamma_p^C + 3\delta_p^C$ were calculated for the outer s and p shells of these noble-gas atoms. The numerical calculations of the electron wave functions and matrix elements in the Hartree-Fock (HF) approximation and in the RPAE both in the ''length'' and ''velocity'' forms were performed using standard codes [42]. In our RPAE calculations considered below the summation and integration over intermediate states in the matrix form of Eq. (12) include three nearest discrete excited levels and 55 continuum states.

A. He 1*s* shell

Multielectron correlation effects have been found to be unimportant in the calculation of the total photoionization cross sections of the He 1s shell [43]. Consistent with this finding, Fig. 1 demonstrates that our HF-L and RPAE results for the nondipole asymmetry parameter γ_s^C for the 1s shell agree excellently over the entire photoelectron energy range, implying that the multielectron correlation effects are also insignificant in the calculation of γ_s^C for the He 1s shell. Only the HF-L (represented simply as HF) result is shown in Fig. 1 because the HF-L and HF-V results are almost identical. The electron wave functions in this case are close to hydrogenlike wave functions. The potential field acting upon the outgoing photoelectron in He^+ is very close to the pure Coulombic one. Therefore, the behavior of the nondipole asymmetry parameter γ_s^C as a function of ϵ increases monotonically, and is everywhere positive.

B. Ne 2*s* subshell

The results for $\gamma_s^C(\epsilon)$ for the 2s-shell of Ne are given in Fig. 2. The multielectron correlations in this case are considerably more important than in He. At and near threshold the HF and RPAE results agree excellently, indicating the unimportance of the multielectron correlation effects in this energy range. However, around the maximum and beyond the minimum, the HF and RPAE results differ significantly, demonstrating the importance (onset) of multielectron correlations. Also as ϵ increases beyond the minimum, the HF-V result deviates from the HF-L one, and eventually merges with the RPAE result near $\epsilon = 1.5$ keV. This supports the well-known fact that sometimes the HF-V result is more reliable when compared with the HF-L one.

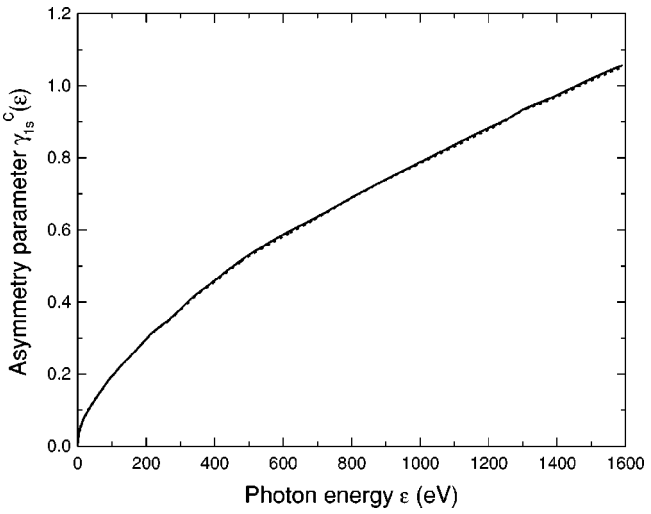

FIG. 1. Nondipole asymmetry parameter γ_s^C for the 1s subshell photoionization of He as a function of the photoelectron energy. Hartree-Fock results in the length HF-L and velocity HF-V formulations are presented (dashed curve) together with those of the RPAE (solid curve).

The ϵ dependence of γ_s^C in Ne is essentially different from that for a hydrogenlike atom. The function $\gamma_s^C(\epsilon)$ changes its sign near the photoionization threshold. The HF

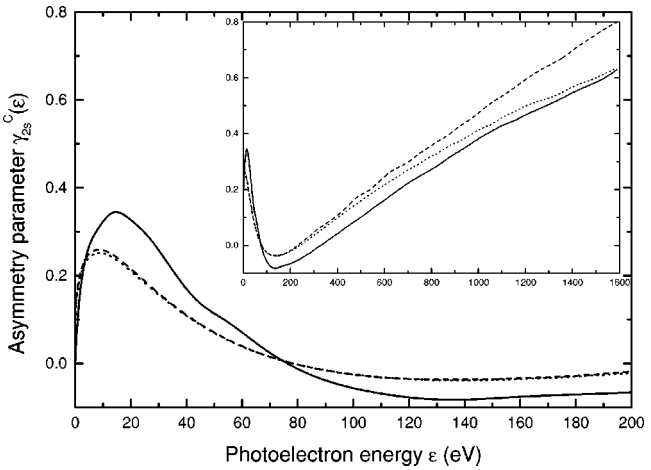

FIG. 2. Nondipole asymmetry parameter γ_s^C for the 2s subshell photoionization of Ne as a function of the photoelectron energy. Hartree-Fock results in the length HF-L (long-dashed curve) and velocity HF-V (short-dashed curve) formulations are compared with those of the RPAE (solid curve).

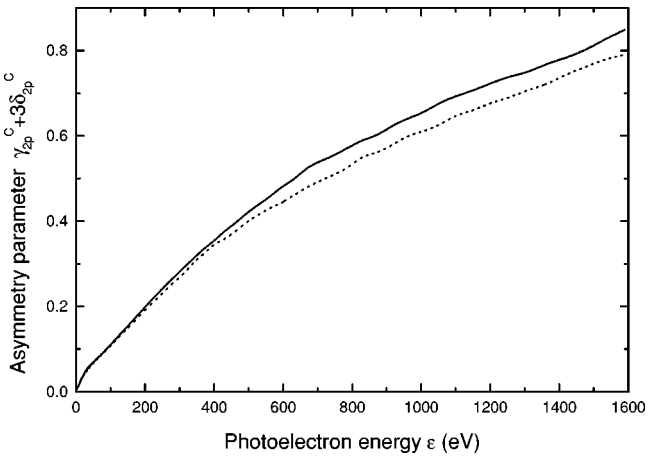

FIG. 3. Nondipole asymmetry parameter ($\gamma_p^C+3\,\delta_p^C$) for the Ne $2p$ subshell photoionization as a function of the photoelectron energy. Only the Hartree-Fock length (dashed curve) in this figure and throughout the subsequent figures is compared with the RPAE (solid curve).

curves go through zero twice. The first zero at $\epsilon\approx 78$ eV is located where the function $\cos(\delta_2-\delta_1)$ in Eq. (8) is equal to zero. The second zero at $\epsilon\approx 244$ eV is due to the sign variation of the quadrupole matrix element q_2.

In RPAE calculations of the dipole matrix elements D_1 all excitations from the $1s$, $2s$ shells to $n(\epsilon)p$ states, and from the $2p$ level to $n(\epsilon)s$ and $n(\epsilon)d$ states, are included. Also in calculations of the quadrupole matrix elements Q_2 all transitions, namely $1s-n(\epsilon)d$, $2s-n(\epsilon)d$, $2p-n(\epsilon)p$, and $2p-n(\epsilon)f$, are simultaneously taken into account. Both the dipole and quadrupole transitions involve a coupled four-channel problem. The RPAE curve in Fig. 2 is close to zero at the $2s$ photoionization threshold. The location of the first zero by the RPAE calculation coincides with that for HF curves. For this electron energy the imaginary parts of the dipole and quadrupole matrix elements in Eq. (12) are small. Therefore, these zeroes in the HF and the RPAE curves are located at the same energy. The second zero at $\epsilon=337$ eV for the RPAE curve is due to the sign variation of the numerator of Eq. (8). As in the HF case, this zero is connected with the behavior of the quadrupole matrix element, viz, the function $Q_2'(\epsilon)$ changes its sign in the vicinity of this energy. The curves obtained are in good agreement with the existing experimental data [7] and calculations [14]. The detailed comparison with these data is presented in our recent paper [43].

C. Ne $2p$ subshell

The calculated $\gamma_p^C+3\,\delta_p^C$ for the Ne $2p$ subshell as a function of ϵ is presented in Fig. 3. In this case, the difference between the HF-L and HF-V data is small; therefore, only the HF-L result is shown, simply as HF. The numerical RPAE procedure in this case is the same as for the Ne $2s$ shell. The function $\gamma_p^C+3\,\delta_p^C$ increases monotonically from zero at the photoionization threshold up to a value of about 0.9 at the photoelectron energy $\epsilon=1.6$ keV. Qualitatively, the behavior of $\gamma_p^C+3\,\delta_p^C$ as a function of photoelectron energy is similar to that of γ_s^C for He or for H. We note that multielectron correlations begin to show for ϵ greater than about 0.4 keV; these effects are still smaller here than they are for the Ne $2s$ shell.

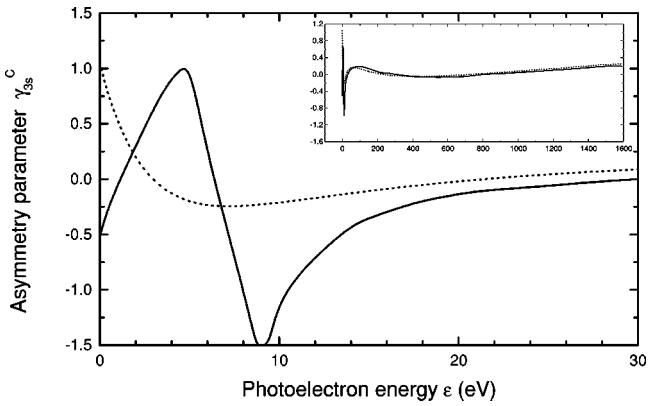

FIG. 4. Nondipole asymmetry parameter γ_s^C for photoionization out of the $3s$ subshell of Ar as a function of the photoelectron energy, calculated in the HF approximation (dashed curve) and the RPAE (solid curve).

D. Ar $3s$ subshell

The RPAE and HF-L values for $\gamma_s^C(\epsilon)$ for the Ar $3s$ subshell are shown in Fig. 4. The insert on this figure represents the function $\gamma_s^C(\epsilon)$ also at high photoelectron energies, up to 1.6 keV. The parameter $\gamma_s^C(\epsilon)$ in the HF approximation is a sign-changing function. The large value of this parameter at the $3s$ threshold results from the fact that d_1 is small and q_2 is large at threshold. The first zero in $\gamma_s^C(\epsilon)$ at $\epsilon\sim 2.3$ eV is located where $\cos(\delta_2-\delta_1)=0$. The second and third zeros at photoelectron energies $\epsilon\approx 21.2$ and $\epsilon\approx 707$ eV, respectively, are due to the sign variation of the one-electron quadrupole matrix element q_2.

In the RPAE calculations for Ar all virtual dipole and quadrupole excitations from the $3p$, $3s$, $2p$, and $2s$ subshells were included, and the RPAE equations for six-coupled channels were solved. The electron correlations in RPAE, particularly the influence of the $3p^6$ subshell, alter the behavior of $\gamma_s^C(\epsilon)$ for the $3s$ electrons dramatically. They change the sign of $\gamma_s^C(\epsilon)$ at the photoionization threshold and add an extra zero and a maximum in the the RPAE curve. The first zero in $\gamma_s^C(\epsilon)$ is shifted to lower energy, $\epsilon\approx 1.3$ eV. This shift is due to nonzero values of the imaginary parts of the matrix elements D_1'' and Q_2''. The large maximum at $\epsilon\approx 5$ eV, the sign variation at $\epsilon\approx 7.6$ eV, and the minimum at $\epsilon\approx 8.9$ eV are connected with the sign variation of the numerator in Eqs. (8) and (15). The shift of other zeros of the function as compared to the HF curve is due to the contribution of the imaginary parts of the matrix elements D_1'' and Q_2''. Consequently, it is seen that the nondipole asymmetry parameter $\gamma_s^C(\epsilon)$ under the action of RPAE electron correlations becomes a complicated function of ϵ with a rich oscillatory structure. Correlation effects are confined to a narrow photoelectron energy range near threshold.

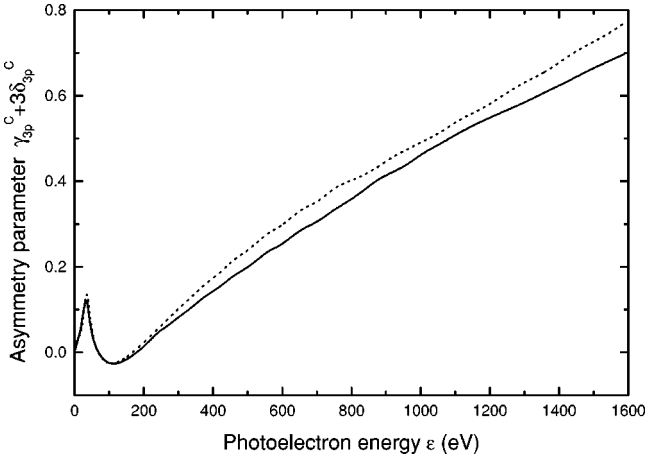

FIG. 5. Nondipole asymmetry parameter $(\gamma_p^C+3\delta_p^C)$ for photoionization out of the $3p$ subshell of Ar as a function of the photoelectron energy, calculated in the HF approximation (dashed curve) and the RPAE (solid curve).

E. Ar 3*p* subshell

Figure 5 shows the results for the outer Ar $3p$ subshell. The multielectron correlations here are not as important as in the $3s$ subshell. Qualitatively, the behavior of $\gamma_p^C+3\delta_p^C$ as a function of ϵ is similar in the one-electron approximation and in the RPAE. The difference between the HF-L and HF-V values is small, hence the use of only the HF-L in the comparison. At the photoionization threshold the values of $(\gamma_p^C+3\delta_p^C)$ are negative, in both HF and RPAE. Zeroes in this function occur at $\epsilon\approx 72$ eV and $\epsilon\approx 170$ eV and are due to the mutual compensation of different terms in the numerator of Eq. (10). Clearly, in the threshold region correlation effects are insignificant, but become noticeable for values of ϵ greater than about 0.35 keV.

F. Kr 4*s* subshell

In the RPAE calculations for the Kr $4s$ shell, five different virtual dipole transitions, namely those from the $4p^6$, $4s^2$, and $3d^{10}$ atomic subshells were included. The quadrupole matrix elements in the RPAE were calculated by solving the RPAE equations with six-coupled channels. The situation is similar to that for the Ar $3s$ state. Figure 6 displays the calculated γ_s^C as a function of ϵ. It is seen that the multielectron correlations play a prominent role near the photoionization threshold. They change the sign of $\gamma_s^C(\epsilon)$ there and add an extra zero and a maximum. The reasons for these changes are the same as in the case of the Ar $3s$ subshell, namely, the sign alteration of D_1' as compared to d_1 and the appearance of nonzero imaginary parts in the matrix elements D_1'' and Q_2''. It is seen that $\gamma_s^C(\epsilon)$ for the Kr $4s$ subshell under the action of multielectron correlations also becomes a function with oscillatory structure. Here, too, correlation effects are limited to the energy region near threshold as in the Ar $3s$ subshell.

G. Kr 4*p* subshell

Interestingly, the ϵ dependence of $(\gamma_p^C+3\delta_p^C)$ for the Kr $4p$ subshell is an oscillating function even in HF. The inclusion of correlations in the Kr $4p$ subshell, as in the case of the Ar $3p$ subshell, has little influence except around the two maxima. The curves in Fig. 7 represent HF-L and the RPAE results, showing their closeness everywhere, except for the photoelectron energy in the vicinity of the peaks, viz, at $\epsilon\approx 35$ eV and $\epsilon\approx 200$ eV. At the latter energy, the HF data are $\approx 28\%$ higher than the RPAE ones. Note that at high ω the values for $(\gamma_p^C+3\delta_p^C)$ in Kr are considerably smaller, by a factor of about four, than the corresponding values in Ar.

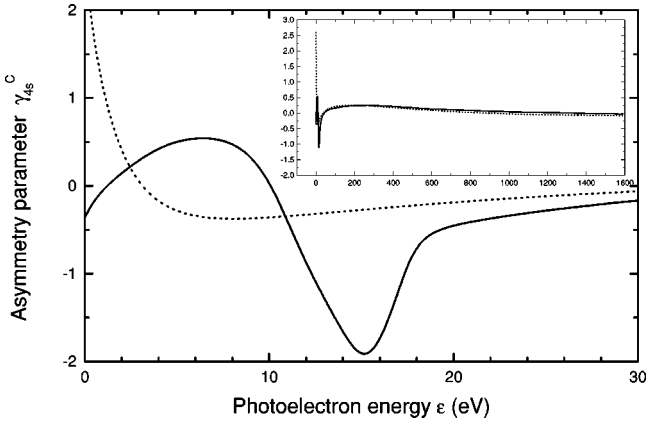

FIG. 6. Nondipole asymmetry parameter γ_s^C for photoionization out of the $4s$ subshell of Kr as a function of the photoelectron energy, calculated in the HF approximation (dashed curve) and the RPAE (solid curve).

H. Xe 5*s* subshell

The RPAE calculation for the Xe $5s$ shell is similar to that for the $4s$ shell and takes into account five channels in the the RPAE equations for the dipole matrix elements and six channels for the quadrupole ones. The analysis for this subshell is similar to that for the Ar $3s$ and the Kr $4s$ subshells. A strong influence of $5p$ electrons is seen in the threshold area [Fig. 8(a)]. Also, the influence of the $4d$ elec-

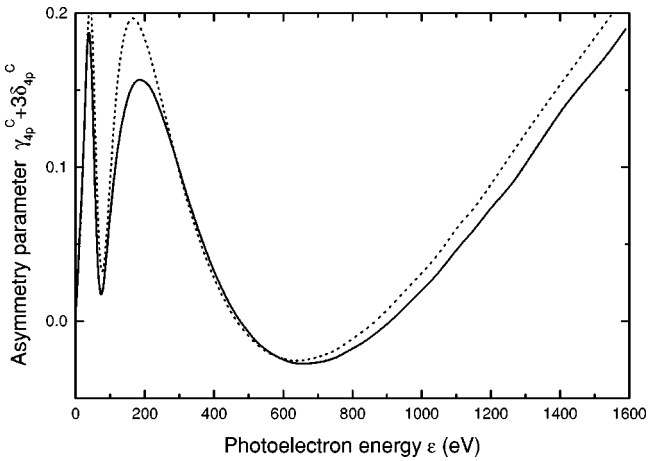

FIG. 7. Nondipole asymmetry parameter $(\gamma_p^C+3\delta_p^C)$ for photoionization out of the $4p$ subshell of Kr as a function of the photoelectron energy, calculated in the HF approximation (dashed curve) and the RPAE (solid curve).

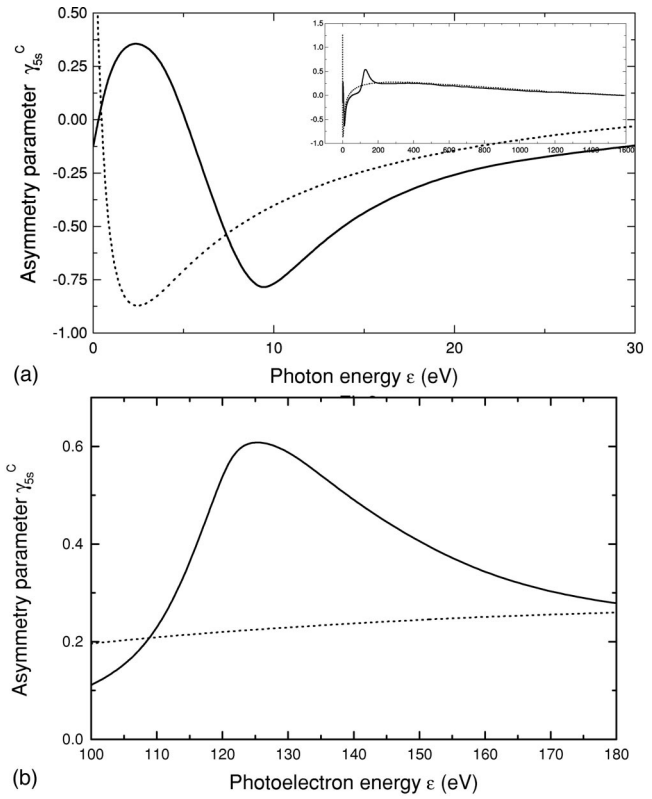

FIG. 8. Nondipole asymmetry parameter γ_s^C for photoionization out of the 5*s* subshell of Xe as a function of the photoelectron energy, calculated in the HF approximation (dashed curve) and the RPAE (solid curve). (a) Near the 5*s* threshold and (b) near the 4d threshold.

trons at 100–150 eV is prominent as depicted in Fig. 8(b). Multielectron correlations strongly alter $\gamma_s^C(\epsilon)$ near the photoionization threshold, changing its sign. Besides, the RPAE correlations add an extra zero and two extra maxima at about $\epsilon \approx 2.5$ and 125 eV, respectively, in the RPAE curve. The reasons for these changes are the same as in the case of the Ar and Kr *s* subshells, except that the maximum at about 125 eV is due to the influence of the 4*d* electrons. In this case also, we have demonstated that the multielectron correlations strongly affect the asymmetry parameter $\gamma_s^C(\epsilon)$ which becomes an oscillatory function of ϵ.

I. Xe 5*p* subshell

Figure 9 demonstrates the ϵ dependence of $(\gamma_p^C + 3\delta_p^C)$ for the Xe 5*p* subshell. The role of correlation effects is quite significant between about 25 and 200 eV above threshold. Although qualitatively, the behavior of $(\gamma_p^C + 3\delta_p^C)$ is similar in both the one-electron HF approximation and the RPAE, the quantitative differences are very significant, particularly the size of the first maximum and the position of the minimum. Multielectron correlation effects reduce the size of the HF maximum at $\epsilon \approx 50$ eV to about 0.15, decrease the HF minimum at $\epsilon \approx 100$ eV to about 0.05 as well as shift its position closer to threshold. Beyond about 200 eV multielectron correlations have little effect on the nondipole parameters.

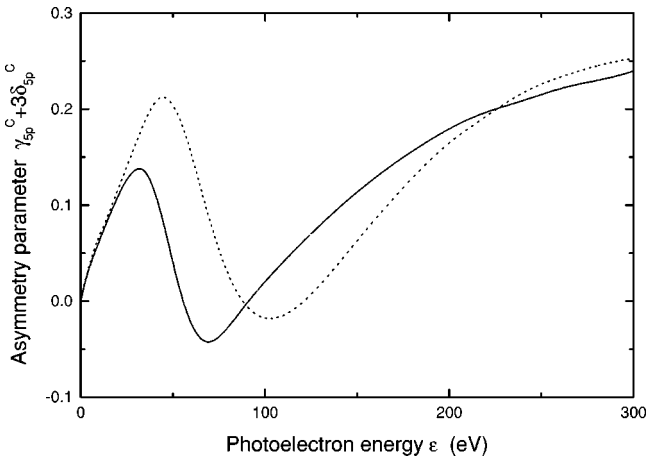

FIG. 9. Nondipole asymmetry parameter $(\gamma_p^C + 3\delta_p^C)$ for photoionization out of the 5*p* subshell of Xe as a function of the photoelectron energy, calculated in the HF approximation (dashed curve) and the RPAE (solid curve).

IV. CONCLUSION AND DISCUSSION

In this paper we have investigated the effects of multielectron correlations on the nondipole asymmetry parameters of the *s* and *p* subshells of the noble-gas atoms by comparing the results of the one-electron HF approximation and the RPAE. Our results cover the photoelectron energy range from the photoionization thresholds to 1.6 keV. Overall, we found that multielectron correlations are significant or mildly so for both the *s* and *p* subshells of all the noble-gas atoms but He. This conclusion supports once more previous findings that the photoionization processes in these atomic subshells are of a collective nature. Therefore, their correct description is generally not possible within the framework of a one-electron approximation such as the HF approximation used here.

Most interesting and revealing, particularly for experimental investigation, is that near the photoionization thresholds the nondipole parameters γ_s^C and $(\gamma_p^C + 3\delta_p^C)$ for the *s* and *p* subshells, respectively, of the noble-gas atoms exclusive of the He 1*s* subshell, are characterized by oscillatory structures as a function of the photoelectron energy. These oscillations are sensitive to multielectron correlations, except those for the Ar 3*p* subshell, as evident from Figs. 2, 4, and 6–9. As the photoelectron energy increases beyond about 300 eV, multielectron correlation effects diminish considerably on the *s* and *p* subshells of Kr and Xe, while these effects linger on for Ne and Ar up to 1.6 keV, as can be seen by comparing the HF and RPAE results. The 1*s* subshell of the lightest noble-gas atom He is, however, unaffected by multielectron correlations regardless of the energy, as already discussed.

ACKNOWLEDGMENTS

The work of A.S.B. was supported by NSF-CREST Grant No. HRD No. 9632844 and in part by Award No. ZP2-2123

of the U.S. Civilian Research & Development Foundation for the Independent States of the Former Soviet Union (CRDF). A.S.B. acknowledges the hospitality of the Center for Theoretical Studies of Physical Systems, Clark Atlanta University (Atlanta, Georgia). A.Z.M. and Z.F. are supported by DOE, Division of Chemical Sciences, Office of Basic Energy Sciences, Office of Energy Research, and NASA-PACE.

[1] G. Rakavy and A. Ron, Phys. Rev. **159**, 50 (1967).
[2] M. O. Krause, Phys. Rev. **177**, 151 (1969).
[3] F. J. Wuilleumier and M. O. Krause, Phys. Rev. A **10**, 242 (1974).
[4] U. Becker, D. Szostak, H. G. Kerkhoff, M. Kupsch, B. Langer, R. Wehlitz, A. Yagishita, and T. Hayaishi, Phys. Rev. A **39**, 3902 (1989).
[5] R. C. C. Perera, Nucl. Instrum. Methods Phys. Res. A **319**, 277 (1992).
[6] B. Krässig, M. Jung, D. S. Gemmell, E. P. Kanter, T. LeBrun, S. H. Southworth, and L. Young, Phys. Rev. Lett. **75**, 4736 (1995); *17th Conference on X-ray and Inner-Shell Processes, Hamburg, Germany*, edited by R. L. Johnson, H. Schmidt-Bocking, and B. F. Sonntag AIP Conf. Proc. No. 389 (AIP, Woodbury, New York, 1997), p. 659.
[7] O. Hemmers, G. Fisher, P. Glans, D. L. Hansen, H. Wang, S. B. Whitfield, R. Wehlitz, J. C. Levin, I. A. Sellin, R. C. C. Perera, E. W. B. Dias, H. S. Chakraborty, P. C. Deshmukh, S. T. Manson, and D. W. Lindle, J. Phys. B **30**, L727 (1997).
[8] N. L. S. Martin, D. B. Thompson, R. P. Bauman, C. D. Caldwell, M. O. Krause, S. P. Frigo, and M. Wilson, Phys. Rev. Lett. **81**, 1199 (1998).
[9] P. Auger and F. Perrin, J. Phys. Radium **6**, 93 (1927).
[10] J. W. Cooper, Phys. Rev. A **42**, 6942 (1990); **45**, 3362 (1992); **47**, 1841 (1993).
[11] A. Bechler and R. H. Pratt, Phys. Rev. A **39**, 1774 (1989); **42**, 6400 (1990).
[12] E. W. B. Dias, H. S. Chakraborty, P. C. Deshmukh, S. T. Manson, O. Hemmers, P. Glans, D. L. Hansen, H. Wang, S. B. Whitfield, D. W. Lindle, R. Wehlitz, J. C. Levin, I. A. Sellin, and R. C. C. Perera, Phys. Rev. Lett. **78**, 4553 (1997).
[13] U. Becker and R. Hentges, *VUV and Soft X-ray Photoionization*, edited by U. Becker and D. A. Shirley (Plenum, New York, 1996).
[14] W. R. Johnson, A. Derevianko, K. T. Cheng, V. K. Dolmatov, and S. T. Manson, Phys. Rev. A **59**, 3609 (1999).
[15] W. R. Johnson and A. Derevianko, At. Data Nucl. Data Tables **73**, 153 (1999).
[16] M. Ya. Amusia, A. S. Baltenkov, Z. Felfli, and A. Z. Msezane, Phys. Rev. A **59**, R2544 (1999).
[17] M. Ya. Amusia, V. K. Dolmatov, and V. K. Ivanov, Pis'ma Zh. Tekh. Fiz. **6**, 1465 (1980) [Sov. Tech. Phys. Lett. **6**, 632 (1980)].
[18] M. Ya. Amusia, V. K. Dolmatov, and V. K. Ivanov, Zh. Tekh. Fiz. **56**, 8 (1986) [Sov. Phys. Tech. Phys. **31**, 4 (1986)].
[19] V. K. Dolmatov and S. T. Manson, Phys. Rev. Lett. **83**, 939 (1999).
[20] M. Ya. Amusia, *Atomic Photoeffect* (Plenum, New York, 1990).
[21] H. A. Bethe and E. E. Salpeter, *Quantum Mechanics of One- and Two-Electron Atoms* (Academic Press, Inc., New York, 1957).
[22] S. T. Manson and D. Dill, in *Electron Spectroscopy: Theory, Techniques, and Applications*, edited by C. R. Brindle and A. D. Baker (Academic, New York, 1978).
[23] V. Schmidt, Rep. Prog. Phys. **55**, 1483 (1992).
[24] C. N. Yang, Phys. Rev. **74**, 764 (1948).
[25] A. Sommerfeld and G. Schur, Ann. Phys. (Leipzig) **4**, 309 (1930).
[26] A. Sommerfeld, *Atombau und Spectrallinien: Wellenmechanische Ergdnzungsband* (Vieweg, Braunschweig, 1928); Wave Mechanics (Methuen, London, 1930).
[27] F. Sauter, Ann. Phys. (Leipzig) **9**, 217 (1931); **11**, 454 (1931).
[28] J. C. Tully, R. S. Berry, and B. J. Dalton, Phys. Rev. **176**, 95 (1968).
[29] M. Peshkin, Adv. Chem. Phys. **18**, 1 (1970).
[30] J. W. Cooper and S. T. Manson, Phys. Rev. **177**, 157 (1969).
[31] H. Pratt, R. D. Levee, R. L. Paxton, and W. Aron, Phys. Rev. A **39**, 898 (1964).
[32] H. Pratt, A. Ron, and H. K. Tseng, Rev. Mod. Phys. **45**, 273 (1973).
[33] K. N. Huang, Phys. Rev. A **22**, 223 (1980); **26**, 3676 (1982).
[34] H. K. Tseng, R. H. Pratt, S. Yu, and A. Ron, Phys. Rev. A **17**, 1061 (1978).
[35] J. Cooper and R. N. Zare, J. Chem. Phys. **48**, 942 (1968).
[36] M. Ya. Amusia, P. U. Arifov, A. S. Baltenkov, A. A. Grinberg, and S. G. Shapiro, Phys. Lett. **47A**, 66 (1974).
[37] M. Ya. Amusia, A. S. Baltenkov, A. A. Grinberg, and S. G. Shapiro, Zh. Éksp. Teor. Fiz. **68**, 28 (1975) [Sov. Phys. JETP **41**, 14 (1975)].
[38] M. Ya. Amusia and V. K. Dolmatov, Zh. Éksp. Teor. Fiz. **79**, 1664 (1980) [Sov. Phys. JETP **52**, 840 (1980)].
[39] M. Ya. Amusia, V. K. Dolmatov, and V. K. Ivanov, Zh. Tekh. Fiz. **36**, 3 (1986) [Sov. Phys. Tech. Phys. **31**, 1 (1986)].
[40] P. S. Shaw, U. Arp, and S. H. Southworth, Phys. Rev. A **54**, 1463 (1996).
[41] M. Jung, B. Krässig, D. S. Gemmell, E. P. Kanter, T. LeBrun, S. H. Southworth, and L. Young, Phys. Rev. A **54**, 2127 (1996).
[42] M. Ya. Amusia and L. V. Chernysheva, *Computation of Atomic Processes, A Handbook for the Atom Programs* (Institute of Physics Publishing, Bristol, 1997).
[43] M. Ya. Amusia, A. S. Baltenkov, L. V. Chernysheva, Z. Felfli, A. Z. Msezane, and J. Nordgren, Phys. Rev. A (to be published).